Journal Pre-proof

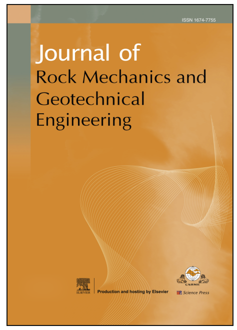

Effects of xanthan gum treatment on sedimentation and consolidation of kaolinite aggregates

Yeong-Man Kwon, Gye-Chun Cho, Ilhan Chang

PII: S1674-7755(25)00097-6

DOI: https://doi.org/10.1016/j.jrmge.2025.01.032

Reference: JRMGE 1957

To appear in: *Journal of Rock Mechanics and Geotechnical Engineering*

Received Date: 6 August 2024

Revised Date: 1 January 2025

Accepted Date: 2 January 2025

Effects of xanthan gum treatment on sedimentation and consolidation of kaolinite aggregates

Yeong-Man Kwon[a], Gye-Chun Cho[b], Ilhan Chang[c,*]

[a] *Department of Civil Engineering, Pukyong National University, Busan 48513, Republic of Korea*
[b] *Department of Civil and Environmental Engineering, Korea Advanced Institute of Science and Technology, Daejeon 34141, Republic of Korea*
[c] *Department of Civil Systems Engineering, Ajou University, Suwon-Si 16499, Republic of Korea*

Abstract
Understanding the sedimentation and simultaneous consolidation behavior of xanthan gum (XG)-biopolymer-treated soils remains a significant research gap in developing environmentally friendly ground-improvement techniques for geotechnical applications. This study addresses this gap by conducting laboratory experiments on kaolinite suspensions with varying XG-to-kaolinite mass ratios (m_b/m_s). The results showed that the XG treatment modified the sedimentation patterns by promoting larger floc formation and accelerated settling. Additionally, the XG treatment enhanced the shear stiffness and shear strength, particularly at shallow depths. At m_b/m_s ratios less than 1%, the volume compression was reduced by the XG; the coefficient of compressibility decreased by 49% at 1% m_b/m_s, and the consolidation was accelerated, as indicated by a 387% increase in the hydraulic conductivity at 0.5% m_b/m_s under the vertical effective stress of 40 kPa. Contrastingly, at m_b/m_s ratios greater than 1%, viscous XG hydrogels clogged pores, resulting in a 45% reduction in the coefficient of consolidation at 2% m_b/m_s under a vertical effective stress of 15 kPa and a 35% decrease in the hydraulic conductivity at 2% m_b/m_s under a vertical effective stress of 40 kPa. These findings underscore the potential of XG treatment in improving the sedimentation and consolidation processes, highlighting its applicability in geotechnical projects, such as dredging, landfilling, and artificial island construction.

Keywords: clays; biopolymer; xanthan gum; consolidation; sedimentation

1. Introduction

Sedimentation and consolidation are closely linked and significantly affect the behavior of soils and structures built upon them (Mitchell and Soga, 2005; Lu et al., 2024). Sedimentation involves the repositioning of soil particles under the influence of gravity, followed by consolidation, which refers to soil compression and a decrease in pore pressure over time. These processes are vital for numerous practical applications, such as environmental remediation (Weng et al., 2024), agriculture (Barciela-Rial and van der Star, 2024), resource management (Néel et al., 2003; Zhang et al., 2024), and geotechnical construction (Yin et al., 2024). Several factors, such as the weight of the overlying sediments, water content, temperature, and pore fluid chemistry, affect sedimentation and consolidation (Hou et al., 2024; Lin et al., 2024), leading to the compaction of soil particles and an increase in their density.

Various materials, such as polyelectrolytes, inorganic coagulants, organic coagulants, and enzymes, are used as flocculants to facilitate soil sedimentation and enhance consolidation behavior (Matilainen et al., 2010; Keeley et al., 2014; Sillanpää et al., 2018). However, these materials are expensive and pose potential environmental hazards (Tang et al., 2016; Zhu et al., 2018). Consequently, organic coagulants, such as tannins, chitosan, enzymes, and composite inorganic–organic coagulants, have gained increasing attention over the last decade (Kwon et al., 2017; Khairul Zaman et al., 2021; Rasheed and Moghal, 2024).

This study aimed to evaluate the feasibility of using a xanthan gum (XG) biopolymer for kaolinite suspensions as an organic coagulant and consolidation aid to address the limitations of conventional flocculants. XG is a versatile substance that has been utilized in various industries, such as food (Chaturvedi et al., 2021), drilling (Quitian-Ardila et al., 2024), concrete production (Wagh and Gandhi, 2024), geotechnical constructions (Anandha Kumar and Sujatha, 2022; Kwon et al., 2023d), and 3D printing (Maierdan et al., 2024). Moreover, XG can form composites with electrically charged biopolymers (Bergmann et al., 2008; Kwon et al., 2023b) and clay (Banu et al., 2020; Vydehi and Moghal, 2022). The interaction between XG and clay surface affects the clay properties, including consistency index, erosion resistance, compressive strength, and shear strength (Wan et al., 2024).

Previous studies have investigated the sedimentation (Yokoi et al., 1996; Tan et al., 2014) and consolidation behaviors (Cabalar et al., 2018) of XG-treated clays. However, studies on XG-treated clays have focused solely on analyzing the separate aspects of sedimentation and consolidation, without addressing the combined process. Delage and Lefebvre (1984) noted that the consolidation properties of the sediments differ markedly from those of uniformly mixed soils. Locat et al. (1996) stated that larger interaggregate pore spaces formed during sedimentation could enhance consolidation by facilitating effective drainage. This indicates a significant knowledge gap regarding the influence of XG on the serial processes of sedimentation and consolidation, which are crucial for the formation of most soil layers.

In this study, the sedimentation and subsequent normal consolidation processes of XG-treated kaolinite were investigated through a combination of sediment deposition in settling columns and consolidation tests using an oedometric cell apparatus. We examined the sedimentation behavior of the XG-treated kaolinites by measuring the settling rate and final sediment density. Furthermore, the changes in vertical effective stress (σ_v') and void ratio (e) during consolidation were analyzed by measuring the shear wave velocity (V_s) in the XG-treated kaolinite specimen. Subsequently, the undrained shear strength (s_u) of the XG-treated kaolinite was analyzed after consolidation. The results of this study have significant potential for analyzing the efficiency of XG in geotechnical engineering applications that utilize suspension-type clays, including those used in dredging, landfills, and artificial island construction.

2. Materials and experimental procedure

2.1 Xanthan gum and kaolinite

The XG used in this study was purchased from Sigma-Aldrich (St. Louis, MO, USA; CAS number: 11138-66-2). XG has the molecular structure $C_{35}H_{49}O_{29}$ and consists of a linear β-D glucose backbone with a negatively charged trisaccharide side chain (Ross-Murphy, 1995). Under static conditions, a small amount of XG can significantly increase the liquid viscosity owing to the repulsive forces between the trisaccharide side chains (Palaniraj and Jayaraman, 2011). The XG utilized herein was a light-yellow-to-beige powder with a Brookfield viscosity ranging from 800 cps to 1200 cps for a 1% solution. A Shimadzu XRF-1800 X-ray fluorescence spectrometer (Shimadzu, Japan) was used to determine the chemical composition of XG, as presented in Table 1.

The clay mineral used in this study was Bintang kaolinite ($Al_2Si_2O_5(OH)_4$) obtained from Belitung Island, Indonesia. Bintang kaolinite, a type of clay with high plasticity, has a liquid limit of 70%, plastic limit of 24%, specific gravity (G_s) of 2.65, mean particle size of 4 μm, and specific surface area of 22 m^2/g.

*Corresponding author. Email: ilhanchang@ajou.ac.kr

Table 1. Chemical composition of xanthan gum.

Analyte	Content
C	87.9%
K	9.13%
Na	2.06%
P	0.29%
Mg	0.22%
S	0.18%
Ca	0.1%
Si	0.06%
Al	0.05%

Kaolinite was oven-dried according to ASTM D2216 (2019). The dried kaolinite (m_s = 140 g) was mixed with varying amounts of XG powder (m_b = 0, 0.14 g, 0.35 g, 0.7 g, 1.4 g, and 2.8 g) to produce the XG-to-kaolinite weight ratios (m_b/m_s) of 0, 0.1%, 0.25%, 0.5%, 1%, and 2%. Instead of the increase in viscosity, m_b/m_s ratios < 2% were selected to observe the effects of the interaction between XG and kaolinite on the soil properties (Sujatha et al., 2021).

2.2 Sedimentation test

The XG-treated kaolinite was then placed in a sedimentation tube of diameter 75 mm (area A = 4417.87 mm^2) with a detachable oedometric cell at the base (Fig. 1). Then, 1400 g of deionized water was added to the tube to obtain a clay slurry with a water content of 1000%. The suspension was slowly mixed using a perforated plunger until a consistent suspension was formed, and the tube was sealed with a thermoplastic film (Parafilm M; Bemis Company, Inc., Bellwood, IL, USA). After hydration for 24 h, the suspension was agitated for 2 min over 60 end-over-end cycles. The tube was placed on a level surface, and the heights of the sediment (h) and suspension were continuously monitored until the sediment reached a constant level, as described in the protocol for the sedimentation test by Palomino and Santamarina (2005).

The experiments were conducted in a controlled environment at room temperature (21±1 °C), to minimize the effects of temperature. The value of e during settling was calculated as follows:

$$e = \frac{v_v}{v_s} = \frac{v_{sed} - v_s}{v_s} = \frac{h \cdot A - (m_s/G_s)}{m_s/G_s} \quad (1)$$

where v_v is the volume of the void spaces, v_s is the volume of the soil, and v_{sed} is the volume of the sediment. Here, the volume of XG is included in v_v rather than in v_s to focus solely on the kaolinite fabrics. Thus, the e of initial sediment was calculated to be 25.7, regardless of m_b/m_s.

2.3 Consolidation test

After the sediment became stabilized, the oedometric cells were gently extracted from the sedimentation tube. The sample within the oedometric cell served as the initial condition for normal consolidation. The sediment specimens with a surface area A = 4417.87 mm^2 were trimmed to a uniform height of 7 cm from the bottom (Fig. 1).

In this study, unimorph-type piezoelectric bender elements (T223-H4CL; Piezo Systems Inc., Woburn, MA, USA) were used to generate and detect shear waves. Each bender element was 12 mm long, 8 mm wide, and 0.6 mm thick. The anode and cathode wires of a coaxial cable were soldered to each side of the element, to form a series configuration. The surfaces of the bender elements were coated with polyurethane for waterproofing and covered with a conductive paste layer to prevent unwanted electromagnetism between the source and receiver elements. The bender elements were firmly mounted on the base of the oedometric cell and underneath the load cap using epoxy resin (Fig. 1).

Prior to loading, the specimens were positioned in an oedometric testing device, and a load cap equipped with a bender element was placed on top of each specimen. The porous plates located at the top and bottom of the specimens allowed pore water to drain in two directions during the loading process. Sequential step loads of 10 kPa, 20 kPa, 30 kPa, and 40 kPa were applied to the specimens to simulate the conditions at the Kwang-Yang Harbor reclamation site (Chang and Cho, 2010) for shallow-depth applications, followed by a final application of a reduced load of 10 kPa. The temperature was maintained at 21 ± 1 °C during the consolidation. V_s was measured for all the specimens in the vertical direction, which was also the loading direction. Shear waves were generated using a signal generator (Agilent 33120A; Keysight, Santa Rosa, CA, USA) with a single input signal of amplitude 5 V and frequency of 5 kHz. The signals received at various depths were stored in a digital oscilloscope (DSOX3024T; Keysight, Santa Rosa, CA, USA), as shown in Fig. 2, and the first arrival of the shear wave was marked as zero after the first bump (Lee and Santamarina, 2005). Fig. 2 shows the decreasing arrival time with increased confinement and inelastic recovery during unloading.

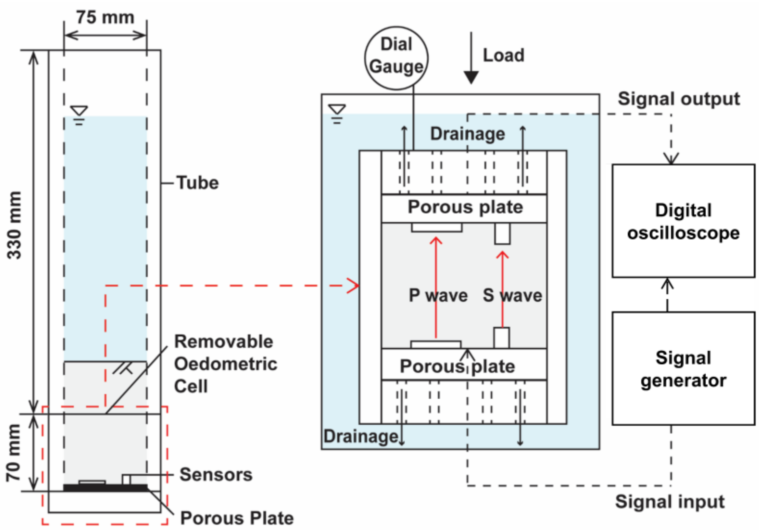

Fig. 1. Experimental setup: Sedimentation tube with a removable oedometric cell (adopted from Chang and Cho (2010)).

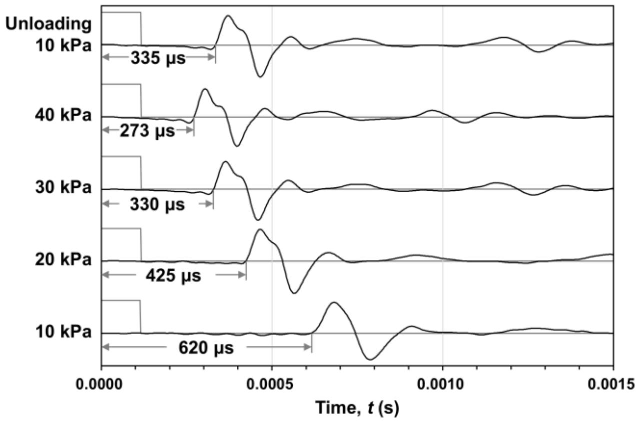

Fig. 2. Example of interpretation of travel time from shear waves.

Once the convergence of V_s and volumetric expansion was achieved, the load cap was detached from the oedometric cell. Laboratory vane shear tests were performed according to ASTM D4648-05 (2007). These tests involved using a vane blade with a length and width of 12.7 mm to ascertain the s_u value of each sample.

2.4 Visual observations: X-ray CT scanning and scanning electron microscopy

An X-ray computed tomography (CT) scanner (X-eye PCT; SEC, Korea) was used to obtain quantitative and spatially resolved information on the X-ray attenuation properties of the scanned regions, providing insight into the flocs and texture of the kaolinite suspension. Therefore, additional sedimentation tests were conducted in tubes of diameter 2.54 cm. Once the sediment height was stabilized, sedimentation tubes containing untreated kaolinite and kaolinite treated with XG at m_b/m_s = 0.5% were placed in the CT machine without further processing. Scanning was performed with a source voltage of 150 kV and a current of 1 A. Each scan produced slice images of 1024 × 1024 pixels, for a total of 1024 thin slices encompassing the entire sediment.

Environmental scanning electron microscopy (ESEM) was utilized with a Model Quattro ESEM (Thermo Fisher Scientific Inc., Waltham, USA), which controlled the water vapor pressure (10–4000 Pa) and relative humidity within the specimen chamber, to examine the microscale interactions between XG and kaolinite after consolidation. Samples of both untreated and XG-treated kaolinite (m_b/m_s = 0 and 1%, respectively) were mounted on an ESEM stub, and the specimen surfaces were exposed to electron beams, with the relative humidity fluctuating between 0 and 100% during the observations.

3. Results and analysis

3.1 Sedimentation and normal consolidation

3.1.1 Sedimentation test

The sedimentation behavior of kaolinite was influenced by the interaction between XG and kaolinite, which varied depending on m_b/m_s (Fig. 3 and Table 2). The untreated kaolinite settled uniformly, forming a distinct interface with the supernatant (bottom left of Fig. 3), which can be classified as the flocculation sedimentation mode, according to Palomino and Santamarina (2005).

With the XG treatment (bottom middle and right of Fig. 3), the sedimentation mode changed from flocculated sedimentation (m_b/m_s = 0, 0.1%) to mixed-mode sedimentation (m_b/m_s = 0.25%, 0.5%) and dispersed sedimentation (m_b/m_s = 1%, 2%). This behavior could be attributed to the XG-induced formation of aggregates (Nugent et al., 2009; Shen et al., 2020; Zhao et al., 2022). When m_b/m_s < 1%, XG formed larger flocs with a larger e, which settled faster than untreated kaolinite because of the increased size and weight (Van der Lee, 2000). However, at $m_b/m_s \geq$ 1%, the supernatant became opaque owing to viscous XG hydrogels (Sun et al., 2007; Chakraborty et al., 2023), making it difficult to distinguish the boundary between the supernatant and the sediment. Meanwhile, the XG packs aggregated more densely or formed their own hydrogels, resulting in a more dispersed settling of soil particles (Kang et al., 2019), leading to a decreased settling rate and a smaller final e.

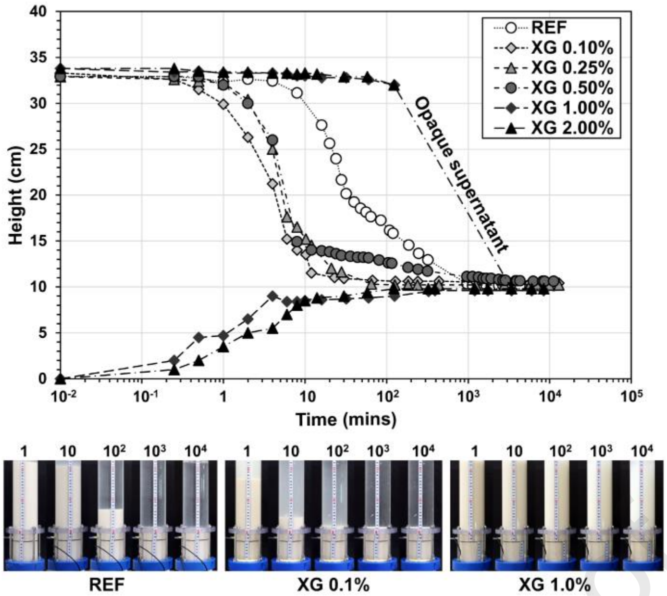

Fig. 3. Variation of sediment height with time.

Table 2. Conditions and results of the sedimentation test

Specimen	Ref (Untreated)			XG-treated		
XG	0	0.1%	0.25%	0.5%	1%	2%
Dry soil (g)	140	140	140	140	140	140
Sedimentation mode*	Flocculation sedimentation	Flocculation sedimentation	Mixed-mode sedimentation	Mixed-mode sedimentation	Dispersed sedimentation	Dispersed sedimentation
Initial void ratio	26	26	26	26	26	26
Final void ratio	7.23	7.47	7.31	7.63	6.41	6.50
Initial settling rate (cm/min) **	0.40	2.58	2.29	2.28		

* Sedimentation mode as defined by Palomino and Santamarina (2005).

** Initial settling rate cannot be measured for the dispersed sedimentation mode.

3.1.2 Consolidation test

Fig. 4 and Table 3 summarize the normal consolidation behaviors of the XG-treated kaolinites. In contrast to the untreated sediment, which had a consistent density throughout the sample, the XG-treated samples demonstrated a denser buildup of aggregates from the bottom (Bottom of Fig. 3), resulting in a density gradient that increased from the bottom and decreased toward the top. Consequently, the large interaggregate pore spaces at the bottom led to a smaller initial *e* for consolidation.

When vertical loading was applied, the XG-treated kaolinite exhibited a larger *e* at the end of consolidation than the untreated kaolinite. The coefficient of compressibility, measured as the ratio of the change in void ratio to the change in vertical effective stress (before loading and at 40 kPa), decreased by 49%, from 0.112 kPa^{-1} (untreated) to 0.057 kPa^{-1} for 1% m_b/m_s. This was attributed to the XG–kaolinite bonds, which resisted compression. This finding contradicts the results of Kwon et al. (2023a), who reported a smaller *e* at the end of consolidation and a higher compressibility for remolded XG-treated kaolinites than untreated kaolinite, particularly for $m_b/m_s \geq 1\%$. This difference in findings could be attributed to the variations in the specimen preparation methods. In a previous study, samples were prepared by mixing kaolinite and XG directly in the laboratory, whereas in this study, samples that underwent sedimentation processes were utilized.

The XG-treated kaolinite exhibited a higher V_s at the end of consolidation when subjected to the vertical loadings of 10 kPa and 20 kPa, even though *e*, which is inversely correlated with V_s (Choo and Burns, 2015), was larger for the XG-treated kaolinite than for the untreated samples. The increase in shear stiffness (i.e., V_s) is mainly attributed to the interaction between XG and kaolinite. In contrast, in the 30–40 kPa range, the untreated samples showed a higher V_s than the XG-treated samples. This is likely due to the dominant effect of the confining pressure, rather than bridge formation by XG, in this range.

3.1.3 Unloading and vane shear test

Table 3 summarizes the *e*, V_s, and s_u values for each specimen after unloading. The lowest volume expansion percentage (1.53%) was observed at 0.1% m_b/m_s, whereas the highest volume expansion percentage (3.21%) was observed at 2% m_b/m_s, suggesting a nonlinear relationship between m_b/m_s and volume expansion. The XG resisted volume expansion at a low m_b/m_s; however, it expanded more than untreated kaolinite with unloading when m_b/m_s exceeded a certain value (i.e., 2% in this study). V_s was lower in XG-treated kaolinites because of their larger *e* than that of untreated kaolinite, whereas untreated kaolinites showed a larger decrease in V_s after unloading (19%) than that of the 0.25%–1% XG-treated specimens (15%–17%). Despite having a lower stiffness and density than the untreated kaolinites, the addition of XG resulted in a higher s_u (Table 3 and Fig. 5). These effects arise from the properties of XG. XG bonds soil particles, enhancing cohesion and increasing shear strength; however, its high flexibility reduces stiffness. Thus, the shear strength and stiffness do not correlate directly; they vary based on the balance between XG bonding and hydrogel flexibility.

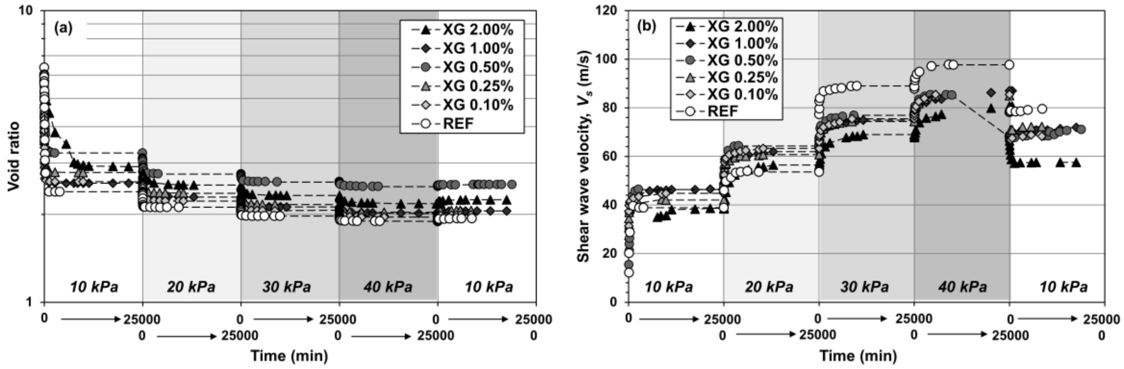

Fig. 4. Variation of (a) void ratio and (b) shear wave velocity during the laboratory consolidation test.

Table 3. Conditions and results of the consolidation test.

Specimen		Ref (Untreated)			XG-treated		
		XG content of 0	XG content of 0.1%	XG content of 0.25%	0.5%	1.0%	2.0%
Consolidation test	*e* before loading*	6.37	4.89	4.91	5.43	4.29	5.45
	e after loading of 10 kPa	2.39	2.59	2.78	2.72	2.56	2.92
	e after loading of 20 kPa	2.11	2.22	2.36	2.23	2.29	2.52
	e after loading of 30 kPa	1.97	2.06	2.16	2.06	2.12	2.32
	e after loading of 40 kPa	1.89	1.96	2.03	1.97	2.02	2.18
	V_s (m/s)=10 kPa	38.83	44.79	42.05	46.36	46.51	38.63
	V_s (m/s)=20 kPa	60.20	63.30	60.74	64.25	61.98	56.41
	V_s (m/s)=30 kPa	79.54	75.41	74.31	76.84	74.89	68.95
	V_s (m/s)=40 kPa	97.70	85.49	84.98	85.20	87.08	80.77
Unloading/Laboratory vane shear test	*e*	1.94	1.99	2.07	2.01	2.06	2.25
	V_s (m/s)	79.47	68.29	72.25	70.99	71.95	57.49
	Undrained shear strength (kPa)	4.00	12.01	11.45	11.76	10.32	7.88

*The initial void ratio before loading was due to the initial confinement applied by the load cap.

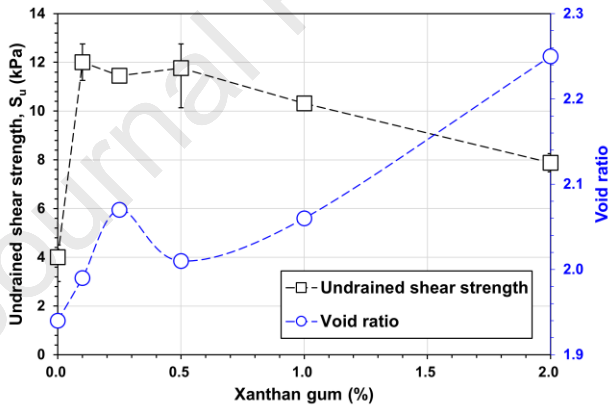

Fig. 5. Effect of xanthan gum treatment on undrained shear strength and void ratio.

3.2 XG effect on consolidation parameters

3.2.1 Vertical effective stress

In Fig. 6, V_s and σ_v' at the end of consolidation were plotted for each applied vertical load. The relationship between V_s and σ_v' is expressed as

$$V_S = \alpha\left(\sigma_v'\right)^{\beta} \quad . \tag{2}$$

where α (m/s) represents V_s at a σ_v' of 1 kPa, whereas β represents the sensitivity of the skeletal shear stiffness to changes in the applied stress. A higher value of α indicates a higher shear stiffness at a shallow depth, whereas a higher β indicates a larger variation in shear stiffness owing to changes in the applied load (Cha et al., 2014).

Compared with the untreated sample, the introduction of XG resulted in an increase in α and a reduction in β. This indicates that, under low vertical loads (i.e., shallow depths), the shear stiffness was enhanced by the XG treatment. However, under higher vertical loads (i.e., deeper depths), the effect of XG on the shear stiffness of the clay fabrics decreased. Consequently, the untreated kaolinite with a smaller *e* exhibited a higher V_s at 30 kPa and 40 kPa than the XG-treated kaolinites. This suggests that the stiffness reinforcement effect provided by the XG is more pronounced at shallow depths (up to 20 kPa). This behavior occurs because, with increasing depth, soil fabric densification becomes the dominant factor influencing stiffness, thereby overshadowing the reinforcement effect due to XG. Note that 0.25% XG exhibited a higher β and lower α than 0.1% XG, which could be attributed to the more effective formation of interparticle bridges at 0.25% XG, which helps maintain stiffness with an increase in the load; however, at 0.1%, XG could primarily be adsorbed onto the particle surfaces without significantly reinforcing the structure.

The remarkable variation in α and β at 0.5% m_b/m_s can be attributed to the balance between the ability of XG to form bridges among kaolinite particles and its influence on the pore spaces within the soil matrix (Theng, 2012). During sedimentation, XG at m_b/m_s less than 1.0% primarily acts as a bridging agent between kaolinite fabrics (Kwon et al., 2023c), enhancing the shear stiffness of the kaolinite sediment at shallow depths (i.e., increased α) . However, as σ_v' increases, these bridges are eventually overcome, leading to the reduced sensitivity of V_s to changes in σ_v'. In contrast, XG treatment at m_b/m_s greater than 1.0% tended to create a viscous hydrogel within the pore spaces, resulting in an increase in e after consolidation (Table 3). This phenomenon led to a decrease in α and an increase in β compared with 0.5% m_b/m_s.

3.2.2 Void ratio (*e*)

The values of e and their corresponding V_s values measured during the consolidation of the XG-treated kaolinites are shown in Fig. 7a. The results showed that, at a similar e, the XG-treated kaolinite resulted in a stiffer sediment formation (i.e., higher V_s). The relationship between e and V_s can be expressed as follows:

$$e = e_{1\mathrm{m/s}} - b_1 \ln V_S \quad (3)$$

where $e_{1\mathrm{m/s}}$ represents the value of e at V_s = 1 m/s, and coefficient b_1 indicates the sensitivity of e to changes in the value of V_s.

A trend of increasing $e_{1\mathrm{m/s}}$ values with XG was observed. However, a decreasing trend was observed at m_b/m_s = 1%, followed by a subsequent increase at m_b/m_s = 2%. This trend suggests that the XG results in an increase in e (i.e., a smaller compression) at low shear-wave velocities (i.e., V_s = 1 m/s; soft soil). The coefficient b_1 increased with m_b/m_s up to 0.5% owing to the presence of XG bridges. However, the b_1 value decreased at 1% XG, potentially because of the formation of a viscous hydrogel within the pore spaces.

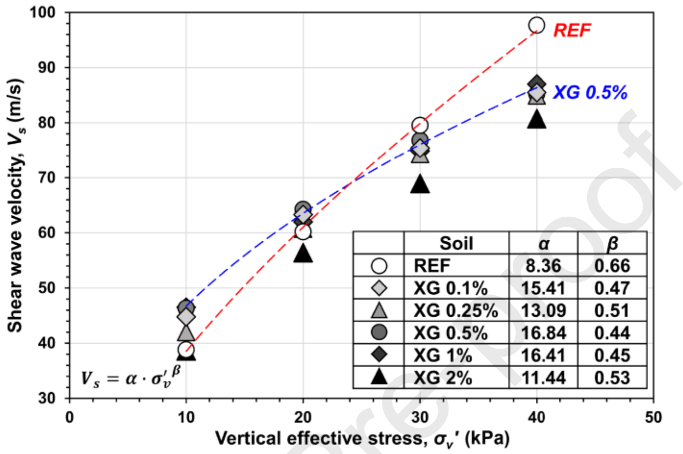

Fig. 6. Correlation between the vertical effective stress and the shear wave velocity from the consolidation test (after loading).

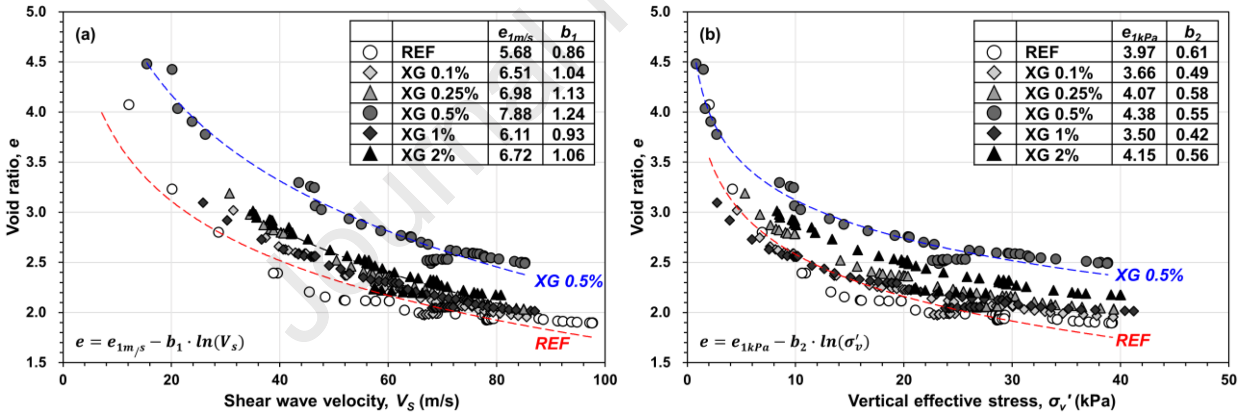

Fig. 7. Variation of void ratio with (a) shear wave velocity and (b) vertical effective stress.

e was plotted against its corresponding σ_v' (Fig. 7b) by substituting Eq. (1) for V_s in Eq. (2) as

$$e = e_{1\mathrm{kPa}} - b_2 \ln(\sigma_v') . \quad (4)$$

where e_{1kPa} represents the e at σ_v' = 1 kPa, and the coefficient b_2 represents the sensitivity of e to changes in σ_v'.

The result demonstrated a larger e at a similar σ_v' with XG treatment, indicating the resistance of XG to the compression of kaolinite by vertical loading. $e_{1\mathrm{kPa}}$ displayed a general increase with increasing m_b/m_s up to 0.5%, followed by a decrease at 1% and an increase again at 2%. This trend indicates that a higher m_b/m_s affects e at a low σ_v'. The coefficient b_2 exhibited a decreasing pattern with increasing m_b/m_s up to 0.1%, followed by an increase at 0.25% and 2%, and a decrease again at 0.5% and 1%. This suggests that the sensitivity of e to changes in σ_v' is influenced by m_b/m_s, with varying effects at different m_b/m_s values.

3.2.3 Coefficient of consolidation

The coefficient of consolidation (C_v) characterizes the ability of the soil to dissipate excess pore water pressure and reach a new equilibrium state (Terzaghi et al., 1996). Even under the same vertical loading, C_v can exhibit a nonlinear behavior during consolidation owing to changes in soil fabrics, e, and σ_v'. The C_v, in cm^2/s, at a specific time t, in s, can be evaluated using the variation in specimen height ($H(t)$; in cm) and the degree of consolidation ($U = \sigma_v'(t)/\sigma_v'$) as follows:

$$C_v = \frac{H_{dr}^{\ 2} \cdot T_v}{t} \quad (5)$$

where the length of the maximum drainage path H_{dr} is half of $H(t)$, and the time factor T_V is determined based on (Terzaghi, 1943; Taylor, 1948) as

$$T_v = \frac{\pi}{4}U^2 \quad \text{(for } U \le 0.6\text{)} \tag{6}$$

$$T_v = 1.781 - 0.933\log_{10}\left(100\left(1-U\right)\right) \quad \text{(for } U > 0.6\text{)} \tag{7}$$

The estimated variation of C_v by the change in σ_v' is shown in Fig. 8a. In the early stages of each vertical loading step, the specimens were highly compressible and demonstrated a high hydraulic conductivity (k), resulting in a high C_v, and rearrangement of soil particles. Consequently, the e value of the soil decreased, leading to an increase in C_v. However, as the consolidation continued, the soil became less compressible, and k decreased owing to the reduction in pore space, causing a decrease in C_v as the consolidation decelerated.

The addition of XG with m_b/m_s less than 1% was observed to increase C_v at a similar σ_v', which contradicts the findings of a previous study that reported a decrease in C_v with the addition of XG (Kwon et al., 2023a). This difference could be attributed to the specimen preparation method used in this study (i.e., uniform mixing and sedimentation). During the sedimentation process, kaolinite particles were bridged by XG, resulting in a larger floc diameter. As interaggregate pores are larger than interparticle pores (Zdravkov et al., 2007), consolidation proceeded more rapidly in the XG-treated kaolinite than in the untreated kaolinite. However, when m_b/m_s exceeded 1%, C_v decreased because the pore spaces were filled with viscous XG hydrogels. For instance, at a σ_v' of 15 kPa, compared with the untreated sample (7.08 × 10^{-6} cm^2/s), C_v increased by a maximum of 1933% at 0.25% m_b/m_s (143.94 × 10^{-6} cm^2/s), whereas a 45% decrease was observed at 2% m_b/m_s (3.88 × 10^{-6} cm^2/s).

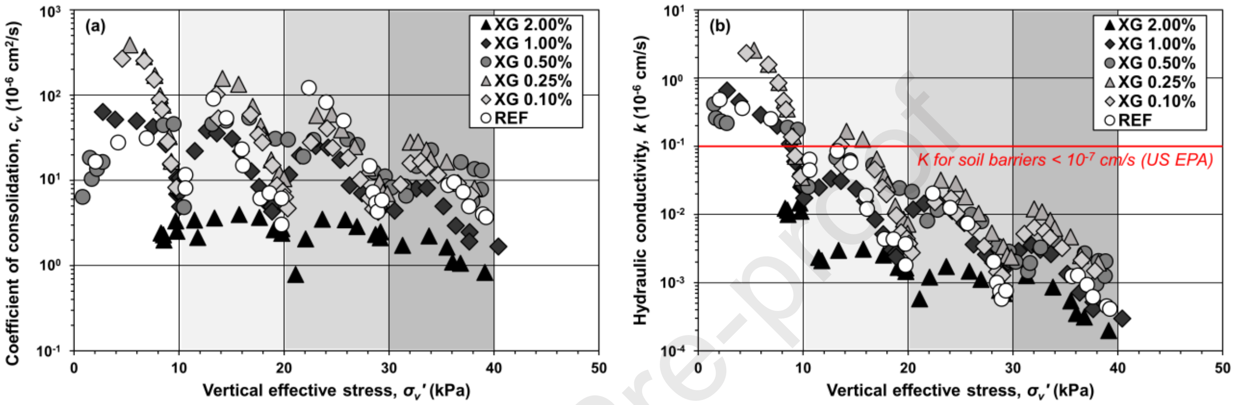

Fig. 8. Variation of (a) coefficient of consolidation and (b) hydraulic conductivity with vertical effective stress.

3.2.4 Hydraulic conductivity

The k, in cm/s, can be expressed as a function of C_v, the coefficient of volume change m_v (cm^2/g), and the unit weight of pore fluid γ_w (g/cm^3) as follows:

$$k = C_v m_v \gamma_w \tag{8}$$

The value of k decreased as σ_v' increased for all the soil specimens (Fig. 8b), which is expected, as sediment consolidation (i.e., decrease in $\boldsymbol{e}$) causes a decrease in k. When XG was added at m_b/m_s <1%, k increased. Specifically, the kaolinite specimens treated with 0.25% XG exhibited the highest k values among the tested soils. In contrast, when m_b/m_s > 1%, the XG hydrogel exhibited pore clogging, resulting in a decrease in k. At a σ_v' of 40 kPa, compared with the untreated sample (5.65 × 10^{-10} cm/s), 0.5% XG resulted in a 387% increase in k (27.53 × 10^{-10} cm/s), whereas 2% XG led to a 35% decrease in k (3.68 × 10^{-10} cm/s). These findings suggest that a low m_b/m_s is recommended for ground reinforcement through rapid consolidation, whereas a higher m_b/m_s is recommended for constructing hydraulic barriers. The reduction in k reached values below the minimum requirement for compacted soil barriers, which is 10^{-7} cm/s or lower.

3.2.5 Visual observation of XG–kaolinite interaction

Fig. 9 shows the interactions between kaolinite and XG. In untreated kaolinite suspensions, the kaolinite particles were uniformly distributed (Fig. 9a), and their random distribution resulted in the sedimentation of individual particles (Fig. 9b and c). However, the introduction of XG resulted in the formation of aggregates of various sizes (Fig. 9d). XG formed a coating around the soil particles (Fig. 9e), creating XG bridges that helped aggregate the particles, which could be observed even after drying (Fig. 9f).

This aggregation occurred because of the ability of XG to act as a bridging agent between the kaolinite particles. XG molecules consist of functional groups, such as hydroxyl (-OH) and carboxylic acid (-COOH) groups, which are capable of forming cation bridges and hydrogen bonds with the surface of kaolinite particles (Barani and Barfar, 2021). Consequently, XG facilitates the formation of interparticle bridges by connecting individual kaolinite particles, leading to the development of larger aggregates. These aggregates differ in density, which leads to a varied sedimentation pattern in which larger aggregates settle first, followed by smaller aggregates. Thus, the XG–kaolinite interaction is governed by the formation of interparticle forces, which induce the bridging and aggregation of kaolinite particles, altering their sedimentation behavior and leading to the structured settling pattern observed in the XG-treated suspensions.

4. Conclusions

In this study, the sedimentation and simultaneous normal consolidation behavior of XG-treated kaolinite was investigated, emphasizing the interaction between XG and kaolinite and its influence on soil engineering properties, such as settling rate, final sediment density, undrained shear strength, coefficients of consolidation, and hydraulic conductivity.

The experimental results demonstrated that the XG treatment significantly influenced the sedimentation and simultaneous normal consolidation processes, and the extent of influence varied based on the XG-to-kaolinite mass ratio (m_b/m_s). Specifically, at lower XG contents (m_b/m_s <1%), XG acted as a bridging agent, forming loose and larger flocs, accelerating sedimentation, enhancing shear stiffness, resisting compression, and promoting rapid consolidation. For instance, at 0.5% m_b/m_s, the hydraulic conductivity increased by 387% (under vertical effective stress of 40 kPa), whereas the coefficient of compressibility decreased by 49% compared with those of the untreated samples. These results highlight the effectiveness of XG in promoting both rapid consolidation and reduced compression at lower dosages.

In contrast, higher XG contents (m_b/m_s ≥1%) led to the formation of viscous hydrogels, which clogged pores, resulting in reductions in the coefficient of consolidation by 45% at 2% m_b/m_s under a vertical effective stress of 15 kPa, and a 35% decrease in the hydraulic conductivity at 2% m_b/m_s under a vertical effective stress of 40 kPa. This demonstrates that, while higher XG concentrations may reduce permeability, they also limit consolidation effectiveness.

This study highlights the potential of XG as a sustainable alternative to synthetic chemical additives in geotechnical engineering, particularly for soil stabilization, land reclamation, and hydraulic barrier construction. The ability of XG to enhance consolidation and improve shear strength while controlling hydraulic conductivity provides practical advantages for ground reinforcement and soft soil treatment.

To expand the applicability of this study's findings, several considerations need to be addressed. The experiments were conducted under controlled laboratory conditions without considering changes in salinity, groundwater chemistry, or temperature fluctuations. Additionally, the long-term stability of XG-treated sediments remains unclear and warrants further investigation. Furthermore, the focus on kaolinite limits the generalizability of the results to other soil types with varying mineralogical and physical characteristics.

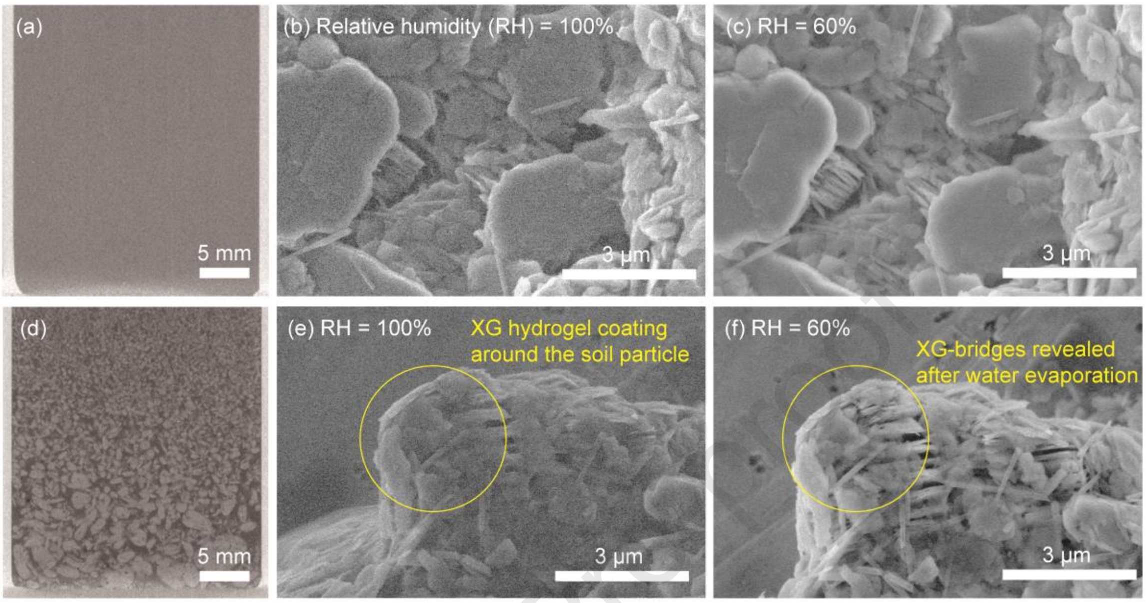

Fig. 9. Visual analysis of kaolinite suspensions: (a) X-ray CT scan of uniform kaolinite suspension (in grey) without XG treatment, ESEM images of untreated kaolinite at the relative humidities of (b) 100% and (c) 60%, (d) X-ray CT scan of XG–kaolinite aggregates (in grey) in deionized water (in black), and ESEM images of XG-treated kaolinite at the relative humidities of (e) 100% and (f) 60%.

Future research should investigate the comparative effects of alternative biopolymers, such as chitosan or guar gum, on sedimentation and consolidation processes. Expanding the scope to include diverse soil types would offer a more comprehensive understanding of biopolymer-soil interactions. Field-scale studies under realistic conditions and long-term assessments of durability, biodegradation, and environmental impacts of biopolymer-treated soils are essential.

Funding

This study was supported by the National Research Foundation of Korea (NRF) grant funded by the Korean government (MSIT) (Grant No. 2022R1A2C2091517).

Declaration of competing interest

The authors declare that they have no competing financial interests or personal relationships that may have influenced the work reported in this study.

Data availability

Data will be made available on request.

List of notations

XG	xanthan gum biopolymer
m_s	weight of kaolinite (g)
m_b/m_s	weight ratio of xanthan gum to kaolinite (%)
A	area of sedimentation tube (m^2)
h	sediment height (mm)
e	void ratio
V_s	shear wave velocity (m/s)
s_u	undrained shear strength (kPa)
σ_v'	vertical effective stress (kPa)
C_v	coefficient of consolidation (cm^2/s)
k	hydraulic conductivity (cm/s)

References

Anandha Kumar, S., Sujatha, E.R., 2022. Assessing the potential of xanthan gum to modify in-situ soil as baseliners for landfills. Int. J. Environ. Sci. Technol. 19(11), 10613-10624.

ASTM D4648-05, 2007. Standard test method for laboratory miniature vane shear test for saturated fine-grained clayey soil. ASTM International, West Conshohocken, PA, USA.

ASTM D2216-19, 2019. Standard test methods for laboratory determination of water (moisture) content of soil and rock by mass. ASTM International, West Conshohocken, PA, USA.

Banu, H.A.T., Karthikeyan, P., Vigneshwaran, S., Meenakshi, S., 2020. Adsorptive performance of lanthanum encapsulated biopolymer chitosan-kaolin clay hybrid composite for the recovery of nitrate and phosphate from water. Int. J. Biol. Macromol. 154, 188-197.

Barani, O.R., Barfar, P., 2021. Effect of xanthan gum biopolymer on fracture properties of clay. Journal of Materials in Civil Engineering 33(1), 04020426.

Barciela-Rial, M., van der Star, W., 2024. Desalination of dredged sediments for beneficial use: A case of study for raising agricultural peatlands. J. Soils Sediments. 24(12), 3854-3862.

Bergmann, D., Furth, G., Mayer, C., 2008. Binding of bivalent cations by xanthan in aqueous solution. Int. J. Biol. Macromol. 43(3), 245-251.

Cabalar, A.F., Awraheem, M.H., Khalaf, M.M., 2018. Geotechnical properties of a low-plasticity clay with biopolymer. J. Mater. Civ. Eng. 30(8), 04018170.
Cha, M., Santamarina, J.C., Kim, H.-S., Cho, G.-C., 2014. Small-strain stiffness, shear-wave velocity, and soil compressibility. J. Geotech. Geoenviron. Eng. 140(10), 06014011.
Chakraborty, S., Dutta, B., Ghosh, N., Halder, S., Chatterjee, R., Sengupta, S., Pal, S., Bandyopadhyay, A., 2023. Strategic grafting of poly metac and polyacrylamide onto xanthan gum for flocculating kaolin at lower concentration. Mater. Today Commun. 34, 105091.
Chang, I., Cho, G.-C., 2010. A new alternative for estimation of geotechnical engineering parameters in reclaimed clays by using shear wave velocity. Geotech. Test. J. 33(3), 171-182.
Chaturvedi, S., Kulshrestha, S., Bhardwaj, K., Jangir, R., 2021. A review on properties and applications of xanthan gum, in: Vaishnav, A., Choudhary, D.K. (Eds.), Microbial polymers: Applications and ecological perspectives. Springer Singapore, Singapore, pp. 87-107.
Choo, H., Burns, S.E., 2015. Shear wave velocity of granular mixtures of silica particles as a function of finer fraction, size ratios and void ratios. Granul. Matter. 17(5), 567-578.
Delage, P., Lefebvre, G., 1984. Study of the structure of a sensitive champlain clay and of its evolution during consolidation. Can. Geotech. J. 21(1), 21-35.
Hou, C.-l., Ma, X.-y., Kang, X., 2024. Effects of salt and ph on microstructure and physico-mechanical behaviors of clay sediments：a references review. Mar. Georesour. Geotechnol. 42(6), 736-766.
Kang, X., Xia, Z., Chen, R., Sun, H., Yang, W., 2019. Effects of inorganic ions, organic polymers, and fly ashes on the sedimentation characteristics of kaolinite suspensions. Appl. Clay Sci. 181, 105220.
Keeley, J., Jarvis, P., Judd, S.J., 2014. Coagulant recovery from water treatment residuals: A review of applicable technologies. Crit. Rev. Environ. Sci. Technol. 44(24), 2675-2719.
Khairul Zaman, N., Rohani, R., Izni Yusoff, I., Kamsol, M.A., Basiron, S.A., Abd Rashid, A.I., 2021. Eco-friendly coagulant versus industrially used coagulants: Identification of their coagulation performance, mechanism and optimization in water treatment process. Int. J. Environ. Res. Public Health. 18(17).
Kwon, Y.-M., Chang, I., Cho, G.-C., 2023a. Consolidation and swelling behavior of kaolinite clay containing xanthan gum biopolymer. Acta Geotech.
Kwon, Y.-M., Chang, I., Cho, G.-C., 2023b. Xanthan biopolymer-based soil treatment effect on kaolinite clay fabric and structure using xrd analysis. Sci. Rep. 13(1), 11666.
Kwon, Y.-M., Im, J., Chang, I., Cho, G.-C., 2017. E-polylysine biopolymer for coagulation of clay suspensions. Geom. Eng. 12(5), 753-770.
Kwon, Y.-M., Kang, S.-J., Cho, G.-C., Chang, I., 2023c. Effect of microbial biopolymers on the sedimentation behavior of kaolinite. Geom. Eng. 33(2), 121-131.
Kwon, Y.-M., Moon, J.-H., Cho, G.-C., Kim, Y.-U., Chang, I., 2023d. Xanthan gum biopolymer-based soil treatment as a construction material to mitigate internal erosion of earthen embankment: A field-scale. Constr. Build. Mater. 389, 131716.
Lee, J.S., Santamarina, J.C., 2005. Bender elements: Performance and signal interpretation. J. Geotech. Geoenviron. Eng. 131(9), 1063-1070.
Lin, C., Bao, R., Zhu, L., Hu, R., Ji, J., Yu, S., 2024. Surface sediment erosion characteristics and influencing factors in the subaqueous delta of the abandoned yellow river estuary. Mar. Geol. 468, 107219.
Locat, J., Trembaly, H., Leroueil, S., 1996. Mechanical and hydraulic behaviour of a soft inorganic clay treated with lime. Can. Geotech. J. 33(4), 654-669.
Lu, M., Zheng, Y.-Y., Yin, Z.-Y., 2024. From sedimentation to consolidation of kaolinite: A molecular dynamic study. Comput. Geotech. 170, 106285.
Maierdan, Y., Zhao, D., Chokshi, P.H., Garmonina, M., Kawashima, S., 2024. Rheology, 3d printing, and particle interactions of xanthan gum-clay binder for earth concrete. Cem. Concr. Res. 182, 107551.
Matilainen, A., Vepsäläinen, M., Sillanpää, M., 2010. Natural organic matter removal by coagulation during drinking water treatment: A review. Adv. Colloid Interface Sci. 159(2), 189-197.
Mitchell, J.K., Soga, K., 2005. Fundamentals of soil behavior, 3rd ed. John Wiley & Sons, Hoboken, NJ, USA.
Néel, C., Bril, H., Courtin-Nomade, A., Dutreuil, J.-P., 2003. Factors affecting natural development of soil on 35-year-old sulphide-rich mine tailings. Geoderma 111(1), 1-20.
Nugent, R.A., Zhang, G., Gambrell, R.P., 2009. Effect of exopolymers on the liquid limit of clays and its engineering implications. Transp. Res. Rec. 2101(1), 34-43.
Palaniraj, A., Jayaraman, V., 2011. Production, recovery and applications of xanthan gum by xanthomonas campestris. J. Food Eng. 106(1), 1-12.
Palomino, A.M., Santamarina, J.C., 2005. Fabric map for kaolinite: Effects of ph and ionic concentration on behavior. Clays Clay Miner. 53(3), 211-223.
Quitian-Ardila, L.H., Garcia-Blanco, Y.J., Daza-Barranco, L.M., Schimicoscki, R.S., Andrade, D.E.V., Franco, A.T., 2024. Improving the rheological and thermal stability of water-based drilling fluids by incrementing xanthan gum concentration. Phys. Fluids. 36(10).
Rasheed, R.M., Moghal, A.A.B., 2024. Efficacy of crustacean and protein-based biopolymer inclusion on the strength characteristics of organic soil. Int. J. Environ. Sci. Technol. 24(11), 04024249.
Ross-Murphy, S.B., 1995. Structure-property relationships in food biopolymer gels and solutions. J. Rheol. 39(6), 1451-1463.
Shen, C.C., Petit, S., Li, C.J., Li, C.S., Khatoon, N., Zhou, C.H., 2020. Interactions between smectites and polyelectrolytes. Appl. Clay Sci. 198, 105778.
Sillanpää, M., Ncibi, M.C., Matilainen, A., Vepsäläinen, M., 2018. Removal of natural organic matter in drinking water treatment by coagulation: A comprehensive review. Chemosphere 190, 54-71.
Sujatha, E.R., Atchaya, S., Sivasaran, A., Keerdthe, R.S., 2021. Enhancing the geotechnical properties of soil using xanthan gum—an eco-friendly alternative to traditional stabilizers. Bull. Eng. Geol. Environ. 80(2), 1157-1167.
Sun, C., Gunasekaran, S., Richards, M.P., 2007. Effect of xanthan gum on physicochemical properties of whey protein isolate stabilized oil-in-water emulsions. Food Hydrocoll. 21(4), 555-564.
Tan, X., Hu, L., Reed, A.H., Furukawa, Y., Zhang, G., 2014. Flocculation and particle size analysis of expansive clay sediments affected by biological, chemical, and hydrodynamic factors. Ocean Dyn. 64(1), 143-157.
Tang, X., Zheng, H., Teng, H., Sun, Y., Guo, J., Xie, W., Yang, Q., Chen, W., 2016. Chemical coagulation process for the removal of heavy metals from water: A review. Desalination Water Treat. 57(4), 1733-1748.
Taylor, D.W., 1948. Fundamentals of soil mechanics. John Wiley and Sons, New York, NY, USA.
Terzaghi, K., 1943. Theoretical soil mechanics. John Wiley, New York, NY, USA.
Terzaghi, K., Peck, R.B., Mesri, G., 1996. Soil mechanics in engineering practice, 3rd ed. Wiley, Chichester, NY, USA.
Theng, B.K.G., 2012. Formation and properties of clay-polymer complexes, 2nd ed. Elsevier, Amsterdam, Netherlands.
Van der Lee, W.T.B., 2000. Temporal variation of floc size and settling velocity in the dollard estuary. Cont. Shelf Res. 20(12), 1495-1511.
Vydehi, K.V., Moghal, A.A.B., 2022. Effect of biopolymeric stabilization on the strength and compressibility characteristics of cohesive soil. J. Mater. Civ. Eng. 34(2), 04021428.
Wagh, C.D., Gandhi, I.S.R., 2024. Investigations on the performance of xanthan gum as a foam stabilizer and assessment of economic and environmental impacts of foam concrete production. J. Build. Eng. 82, 108286.
Wan, J., Tang, Z., Liu, Y., Xiao, H., Wang, H., 2024. Study on the improvement of clay properties by xanthan gum and its application on ecological slope protection engineering. Environ. Technol. 45(14), 2762-2775.
Weng, Z., Yu, J., Cai, Y., Liu, S., Tu, B., 2024. Chitosan composite alkali-activated geopolymer for solidification/stabilization of copper and chromium contaminated mudflat sediment. J. Environ. Chem. Eng. 12(5), 113408.
Yin, J.-H., Chen, W.-B., Wu, P.-C., Leung, A.Y.F., Yin, Z.-Y., Cheung, C.K.W., Wong, A.H.K., 2024. Field study of a sustainable land reclamation approach using dredged marine sediment improved by horizontal drains under vacuum preloading. J. Geotech. Geoenviron. Eng. 150(11), 04024114.
Yokoi, H., Shiraki, M., Hirose, J., Hayashi, S., Takasaki, Y., 1996. Flocculation properties of xanthan produced by xanthomonas campestris. Biotechnol. Tech. 10(10), 789-792.
Zdravkov, B., Čermák, J., Šefara, M., Janků, J., 2007. Pore classification in the characterization of porous materials: A perspective. 5(2), 385-395.
Zhang, W., Zhang, C., Lei, X., Quintero Olaya, S., Zhu, Y., Zhao, Z., Jensen, S., Williams, D.J., 2024. Instrumented column testing on long-term consolidation and desiccation behaviour of coal tailings under natural weather conditions. Acta Geotech. 19(4), 1891-1909.
Zhao, B., Li, S., Lin, H., Cheng, Y., Kong, X., Ding, Y., 2022. Experimental study on the influence of surfactants in compound solution on the wetting-agglomeration properties of bituminous coal dust. Powder Technol. 395, 766-775.
Zhu, G., Liu, J., Bian, Y., 2018. Evaluation of cationic polyacrylamide-based hybrid coagulation for the removal of dissolved organic nitrogen. Environ. Sci. Pollut. Res. 25(15), 14447-14459.

	Dr. Ilhan Chang is an Associate Professor in the Department of Civil Systems Engineering at Ajou University in the Republic of Korea. He earned his BS (2000), MS (2004), and PhD (2010) in Civil and Geotechnical Engineering from KAIST (Korea Advanced Institute of Science and Technology). Before his current role, Dr. Chang worked as a Senior Researcher at the Korea Institute of Civil Engineering and Building Technology (KICT) and as an academic faculty member at the University of New South Wales (UNSW) in Australia. Dr. Chang and his research team focus on interdisciplinary research in emerging geotechnical engineering areas, including Soil Characterization, Ground Improvement, Soil Erosion and Preservation, Biopolymer-Based Soil Treatment (BPST), Biological/Bio-Inspired Soil Treatment, Anti-Desertification, Hydrogeotechnical Engineering, New Civil Engineering Materials, and Sustainable Urban Development.

Declaration of interests

☒ The authors declare that they have no known competing financial interests or personal relationships that could have appeared to influence the work reported in this paper.

☐ The author is an Editorial Board Member/Editor-in-Chief/Associate Editor/Guest Editor for *[Journal name]* and was not involved in the editorial review or the decision to publish this article.

☐ The authors declare the following financial interests/personal relationships which may be considered as potential competing interests: